Vibration attenuation of dual periodic pipelines using interconnected vibration absorbers

Mohd Iqbal, Mahesh Murugan Jaya, Alireza Ture Savadkoohi, Sébastien Baguet

Vibration attenuation of dual periodic pipelines using interconnected vibration absorbers

Mohd Iqbal[1,2*], Mahesh Murugan Jaya[3], Alireza Ture Savadkoohi[1] and Sebastien Baguet[2]

[1]Univ Lyon, ENTPE, Ecole Centrale de Lyon, CNRS, LTDS, UMR 5513, 69518 Vaulx-en-Velin, France.

[2]Univ Lyon, INSA Lyon, LaMCoS, UMR, CNRS 5259, 69621 Villeurbanne, France.

[3]Politecnico di Torino, Torino, 10129, Italy.

*mohammad.iqbal@entpe.fr

Abstract

Pipelines are crucial elements in various engineering applications. However, unexpected vibrations from different sources can jeopardize the operational performance and potentially damage the piping structures and other connected units. This study explores flexural wave propagation and attenuation characteristics of the pipes supported periodically on a rack. Also, a specific case of a rack with infinite stiffness (simple support) is investigated. The dispersion relations pertinent to pipe rack scenario is obtained through transfer matrix method (TMM) in conjunction with Floquet-Bloch's theorem, and the accuracy of ensuing band gaps (BGs) are confirmed through finite element (FE) models. Following this, the modal analysis is performed to ascertain the minimum number of unit-cells necessary for the FE model to accurately mimic the attenuation and propagation characteristics of the corresponding infinite structure. The findings indicate that a pipe supported on rack displays resonance and Bragg-type BGs, arising from local resonance and spatial periodicity, respectively, while the pipe on simple support exhibits only Bragg-type BGs. To control low-frequency vibrations in dual pipelines placed on the rack, a novel configuration using interconnected dynamic vibration absorbers (DVAs) is proposed. The DVA consisting of two spring-damper units along with a mass is connected across the center of each

span of the two pipelines. The proposed DVA is designed via genetic algorithm-based optimization. It was found that the designed DVA significantly reduces the vibration of the two pipelines. The performance of DVAs improves with an increase in the mass ratio. Additionally, the performance of pipes connected with conventional tuned mass damper (TMD) is evaluated and compared with the proposed DVA. The effectiveness of DVAs is also verified by employing a white Gaussian noise as input. The proposed DVAs are efficient in scenarios involving multiple pipes within a rack, leveraging other pipe's mass, stiffness, and damping properties to mitigate vibrations in the considered pipes.

Keywords

Periodic rack structure, Flexural wave, Dispersion diagram, Dynamic vibration absorbers, Vibration control

Abbreviation	
BG	Band gap
BS	Bragg scattering
DoF	Degree-of-freedom
DVA	Dynamic vibration absorber
FE	Finite element
FFT	Fast Fourier Transform
GA	Genetic algorithm
LR	Local resonance
LB	Lower bound
PB	Pass band
PnCs	Phononic crystals
SDoF	Single-degree-of-freedom
TMD	Tuned mass damper
TMM	Transfer matrix method
UB	Upper bound

1. Introduction

1.1. Background and motivation

Pipes are crucial components in various industries including aerospace, liquified natural gas plants, nuclear plants, chemical plants, water treatment plants, and petroleum industries. They serve as conduits for transferring fluids between processing units and storage tanks. In instances where long pipelines exist, rack structures or columns/piers are used at regular intervals to support them. Such pipelines may encounter vibrations from different factors including machinery, base excitation, explosions, wind, flow-induced turbulence, etc. Over time, these vibrations can lead to instability, fatigue failure, loosening of joints, etc. [1]. Additionally, these vibrations can generate excessive noise, impacting health of workers operating in the vicinity. Therefore, attaining higher stability and vibration control standards in pipes is essential [2].

In recent years, phononic crystals (PnCs) gained significant attention from the research community. PnCs are composite structures made up of a periodic array of scatterers embedded in a host medium. Due to impedance mismatch of scatterers, these structures can block waves within specific frequency ranges, resulting in band gaps (BGs). Waves of other frequencies can freely pass through, and are referred to as pass bands (PBs) [3]. This unique characteristic enables PnCs to work as efficient wave filters, facilitating their application in controlling sound and vibrations. BGs in periodic structures occur either from Bragg scattering (BS) [4] or local resonance (LR) [5]. In the former, BGs arise from multiple scattering of the periodic inclusions, and occur when the unit-cell length L and the wavelength λ are comparable in a periodic structure. The position of n^{th} order BG is determined by the Bragg condition $L = n\left(\frac{\lambda}{2}\right)$ $(n = 1,2,3, \dots)$. Conversely, LR BGs originate from the interaction between elastic waves and localized scattering units, and they are independent of the structural periodicity. Frequency range of LR BG is approximately two orders

of magnitude lower than that from Bragg scattering [6]. By optimally tuning the system properties, LR BGs can be used to effectively control vibration and noise within the targeted frequency range [7–9].

There are several studies that discuss the BGs in structures due to BS [10–14]. Recently, Pelat et al. [15] investigated Bragg-type BG in periodically corrugated beams and concluded that their central frequency and width depend solely on the beam thickness. Ding et al. [16] used the transfer matrix method (TMM) to analyze the BGs behavior in periodic jointed tunnels under the influence of moving load. Zhao et al. [17] introduced PnC beam featuring flexural BGs to control vibrations in the low-frequency range. Sorokin et al. [18] studied BG properties in homogeneous and periodic waveguide via finite element method. Carta et al. [19] considered a bridge as an infinite periodic structure and analyzed the BG characteristics. Shen et al. [4] examined the impact of moving loads and flowing fluid on BGs in fluid-conveying shells placed on elastic foundations using TMM. Guo et al. [20] examined the flexural wave propagation characteristics in periodically orthogonal stiffened plates with holes of varying sizes.

Unlike Bragg BGs, LR BGs arise due to locally resonant units in the systems [21]. This concept has been used to control low-frequency vibrations in various structures like pipes [3,6,22], beams [23–25], plates [26,27], shafts [28,29], and railway tracks [30,31]. Recently, Li et.al [32] designed a system consisting of a double beam with periodically attached resonators to control flexural wave propagation in the low-frequency range. Zhao et al. [33] investigated one-dimensional wave propagation characteristics of metamaterials with double resonators. Lee et al. [34] proposed a metamaterial configuration of a periodic duct for reducing longitudinal vibrations at low frequencies. Xiao et al. [35] studied new metamaterial designs to achieve wide BGs at low frequencies. These systems encompass both monatomic and diatomic configurations using a

combination of negative stiffness absorbers and the rotation of flexural beams amplified by outriggers. Li and Sheng [36] conducted analytical and numerical studies on the BGs in an LR plate featuring a periodic array of single and multi degree-of-freedom (DoF) resonators.

In the context of pipes, Liang et al. [37] explored the flexural-torsional vibration BG characteristics of an eccentric fluid-conveying pipe made of alternating materials along its length. Wu et al. [38] investigated the BG properties of a composite pipeline filled with liquid. The pipeline was composed of alternate materials, and the study analyzed the effects of fluid-structure interaction and material properties on the BG characteristics. Liang and Yang [39] examined the BG behavior of a fluid-conveying pipe and analyzed its dependence on the flow velocity. Yu et al. [40] investigated the attenuation properties of a periodically changing cross-section pipe using TMM. Surface wave attenuation in a shallow buried pipe was studied using both analytical and numerical approach in the frequency domain by Ni et al. [41]. Liang et al. [42] examined the flexural vibration properties of a fluid-conveying PnC pipe using TMM. The study also demonstrated the effects of spinning motion of the pipe on the BGs. Wu et al. [43] analyzed the behavior of torsional vibration in a fluid-filled pipe using the TMM and further studied the effects of pipe wall material and support parameters on BGs. Liang et al. [44] designed a laminated fiber-reinforced composite pipe with piezoelectric actuators periodically attached along its length to excite the phononic BG. A control strategy has been proposed to suppress vibrations in fluid-conveying pipes using periodic acoustic black hole wedges by Bu et al. [45]. Geng et al. [46] explored the flexural BGs in a sleeved PnC pipe in thermal environment and also showed the effects of thermal stresses on the BG properties. Plisson et al. [47] employed numerical and experimental approaches to obtain vibration BG in a bi-material pipe comprising of alternating cross sections.

Another common strategy to control vibration involves incorporating resonators in the host structures. For example, Fernandes et al. [48] studied the influence of resonator mass and fluid flow velocity on the bounding frequencies of BGs in a metamaterial pipe. Lei et al. [6] improved the BG properties of a meta-pipe using negative stiffness SDoF resonators. Liang et al. [49] developed a two-dimensional hybrid BS-LR metamaterial pipe, and demonstrated the influence of flow properties on the BGs. Cai et al. [22] proposed quasi-zero stiffness resonator to control low frequency vibrations in a pipe. Matos et al. [50] explored the flexural BGs in a periodic pipe conveying two-phase intermittent flow. Attenuation characteristics of a pipe attached with local resonators were examined by Borgi et al. [51]. Iqbal et al. [52] analyzed the BGs in a pipe with two DoF resonators under different boundary conditions. The vibration attenuation strength of a uniform pipe equipped with piezoelectric patches was enhanced through the synergistic effects of Bragg scattering and electro-elastic resonance by Lyu et al. [53]. Liu et al. [54] examined the attenuation properties of a metamaterial pipe and found that the effect of axial load on BGs was more significant than that of the fluid pressure. Yu et al. [55] studied the BS and LR BG properties in a periodically supported fluid-conveying pipe under external moving load using TMM. The vibration attenuation properties of a fluid-conveying pipe resting on periodic inerter-based resonant supports were investigated by Sciutteri et al. [56]. Wu et al. [57] analyzed wave propagation in a composite fluid-filled pipe with periodic axial support and dynamic vibration absorbers.

PBs in periodic structures refer to frequency ranges where waves transport energy, leading to noise and vibration. It is essential to control vibrations when they fall in frequency of interest. To address this, various passive control techniques are available. Tuned mass damper (TMD) [58] is a commonly employed control technique in which a secondary mass characterized by a specific

mass ratio μ, is connected to the primary structure via spring-damper elements. TMD absorbs energy from the primary structure, which is subsequently dissipated by its intrinsic damping properties [59]. To achieve optimal control for any specified μ, the stiffness and damping properties of the TMD must be designed appropriately [60]. For this, a significant response of the primary system, usually acceleration or displacement is minimized. Closed-form analytical expressions are available for determining the optimal spring-damper properties of TMDs for simple structures subjected to typical standard excitations [61–63]. Many of these expressions are derived using certain assumptions, limiting their applicability to simple structures [64]. Therefore, in situations involving complex structures or unconventional loading conditions, numerical optimization schemes are employed for designing TMDs [65–67].

Various forms of TMDs are available for controlling vibrations in pipeline systems [65]. Each of these systems includes an external mass along with spring-damper elements with specified properties attached to the pipe for control. Stiffness in such cases is either due to shear or bending strength of the employed elastomer materials [68,69], while damping may arise from various sources such as the impact of the TMD mass against surfaces [66], material damping of elastomers [70], fluid damping of the mass [71], etc. Although conventional TMD systems are efficient, they have a drawback of employing an additional mass with the primary structure, leading to an increase in total mass of the system. It is feasible to utilize any existing mass within the system to serve as an energy dissipation and control mechanisms. Although, the performance of these systems is debatable, they offer a promising, cost-effective and simple method for controlling structure.

1.2. Novelty and core contribution

A theoretical and numerical study of propagation characteristics of flexural waves in a periodic pipe P_1 placed on a rack structure is conducted. The corresponding dispersion relation is derived

employing the TMM in conjunction with Floquet-Bloch's theorem. The resulting BG characteristics are confirmed through a finite element (FE) model. Subsequently, a modal analysis is performed to determine the optimal number of unit-cells needed for the FE model to accurately replicate the BG and PB ranges of the corresponding infinite structure. The study presents a novel approach to control low-frequency vibrations in dual periodic pipeline systems. To control vibrations in a PB, a single-degree-of-freedom (SDoF) dynamic vibration absorber (DVA) is initially attached at the midpoint of each span of the two identical pipes P_1 and P_2, as shown in Fig. 1. The equivalent model is illustrated in Fig. 2(b). Subsequently, to compare the performance of DVA with a conventional SDoF TMD, the latter is installed in each span of both the pipes as shown in Fig. 2(c). Unlike conventional TMD, the proposed DVA has the advantage that only a minimal mass needs to be added to control both pipelines. Detailed optimization studies were conducted to design these systems. The efficiency of the proposed DVAs is verified under a white Gaussian noise input. The proposed concept of DVA is efficient for simultaneously controlling vibrations of multiple pipelines, and can be easily executed in power and process industries. This unique idea of DVA can also be applied in scenarios involving parallel beam type flexural systems such as periodic railway tracks, closely spaced bridges, underwater tunnels, etc.

This paper is organized as follows: Section 2 describes the analytical and numerical model of pipes with rack structure. The analytical dispersion relation is first derived and a FE model is built to validate the former. Subsequently, the vibration control scheme along with their optimal design is discussed. Section 3 presents the results for both uncontrolled and controlled pipe. The main findings of the work including future prospects are summarized in Section 4.

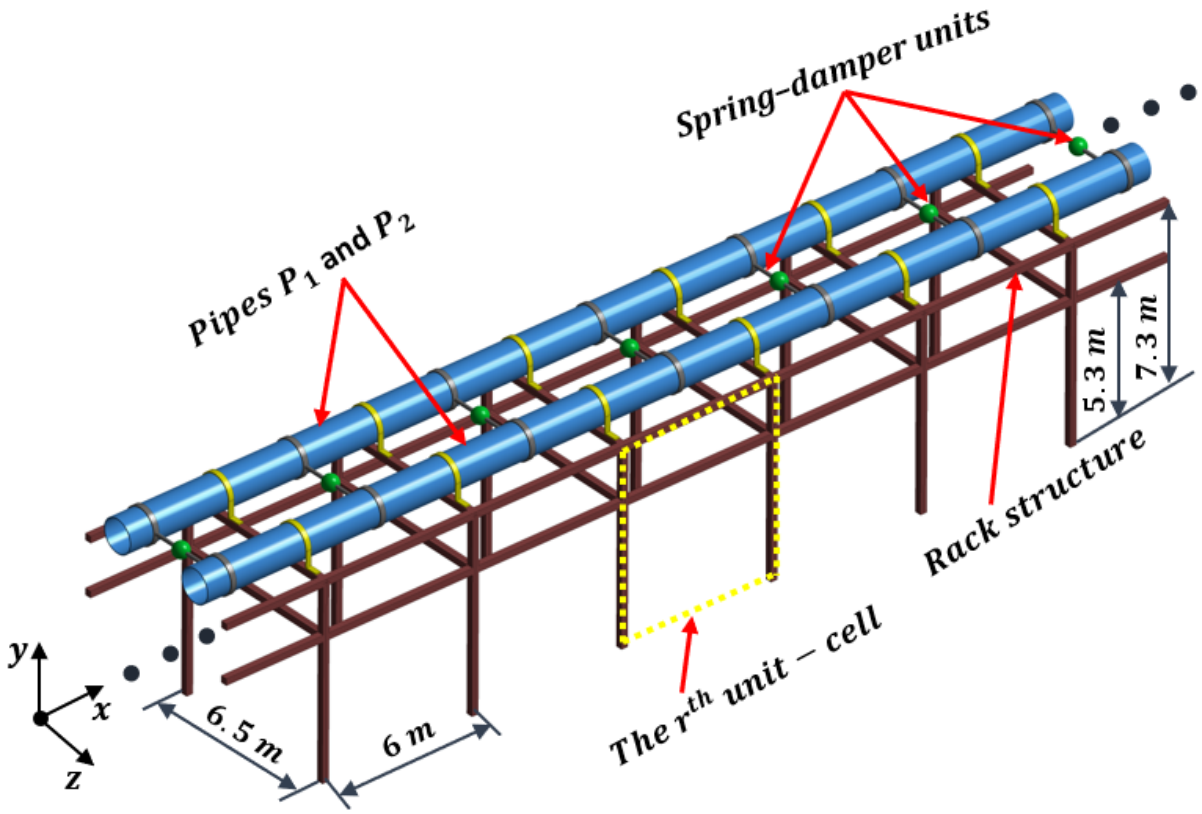

Fig. 1. Pipes P_1 and P_2 of identical properties supported on the rack structure.

2. Analytical and numerical modelling

This section discusses the modelling techniques used for the pipe supported periodically on a rack structure followed by the design of DVA. For this, the pipe-rack structure illustrated in Fig. 1 is utilized. It comprises of two levels, first situated at 5.3 m and the second at 7.3 m from the ground. The distance between two successive columns along the pipe is 6 m, whereas the width of the rack is 6.5 m. More details about this rack can be found in Bursi et al. [72]. The coordinate x, y and z in Fig. 1 respectively represent the longitudinal (along the pipe), lateral and vertical directions.

A 3D FE model of the rack, comprising forty unit-cells, was initially developed. The first predominant mode (along z-axis) was identified at a frequency of 4.5 Hz. An equivalent model of the rack, representing its behavior in the lateral direction, was created as shown in Fig. 2(a). Here,

the lumped mass M_{pr} and stiffness K_{pr} were calculated to replicate the behavior of 3D model for this mode. This resulted in values of $M_{pr} = 2.3\text{E}4$ kg and $K_{pr} = 1.8\text{E}6\ \text{N/m}$. The pipe has an inner diameter of 390.56 mm and an outer diameter of 406.40 mm, with a Young's modulus of $2\text{E}11\ \text{N/m}^2$ and a density of $7800\ \text{kg/m}^3$. A material damping ratio (ξ) of 2% is taken into account for both pipe and the rack. The rack is modelled as a SDoF spring-mass system, and the pipe is modelled using Euler-Bernoulli beam theory. For simplicity, any effects of the fluid flowing through the pipes such as its mass and velocity are neglected in the analysis. The mass of the secondary pipe P_2 that is already present in the rack is not considered in the formulation of dispersion relation of P_1.

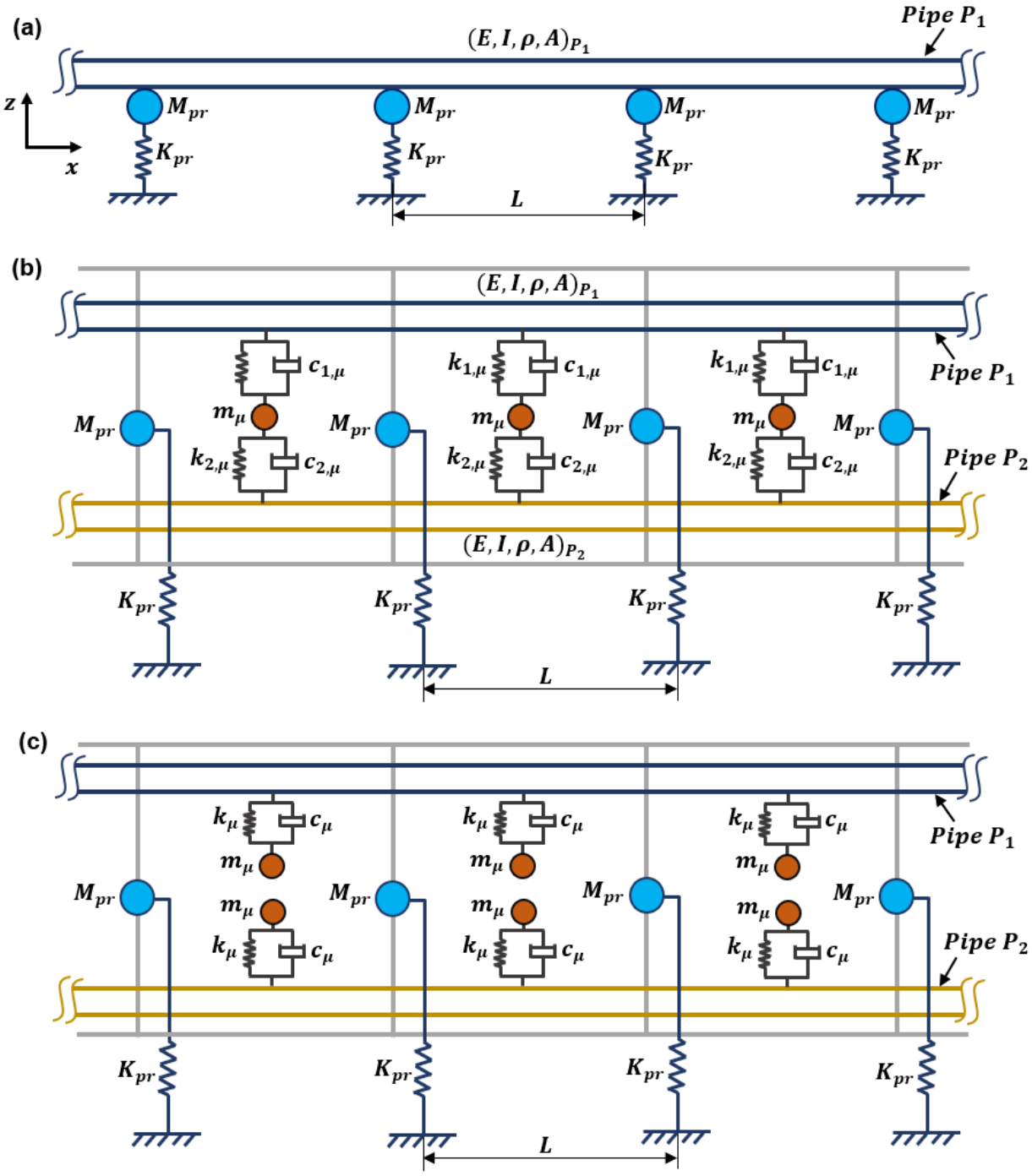

Fig. 2. Equivalent numerical model of Fig. 1: (a) P_1 supported on rack; (b) rack containing two pipes P_1 and P_2 interconnected by dynamic vibration absorbers, and (c) Conventional tuned mass dampers connected to P_1 and P_2.

For controlling specific PB in the pipe, DVA and TMDs are respectively employed as shown in Figs. 2(b) and (c). The DVA consists of an external mass m_μ of mass ratio μ connected to pipe P_1 and P_2 in each span using two sets of spring-damper units ($k_{1,\mu}$, $c_{1,\mu}$ and $k_{2,\mu}$, $c_{2,\mu}$). Similarly, spring–damper properties k_μ and $c_\mu$and mass m_μ is adopted for the conventional TMDs connected to both the pipes. When a particular pipe (say P_1) is subjected to undesirable vibration, the DVA along with other pipe P_2 gets mobilized in controlling vibrations. Since P_2 is connected to P_1, it may sometimes produce undesirable vibration in the former and it has to ensured that this is within the permissible limits. The proposed DVA works identically for both the pipes. However, in case of conventional TMDs, only the TMD associated with the vibrating pipe is activated.

For given pipe dimensions and mass m_μ, optimal properties of spring-damper units of the DVA can be determined. In practice, the DVA can be realized by connecting the pipes to a mass m_μ using spring–damper elements (e.g., steel springs, hydraulic dampers, etc.) with required stiffness and damping properties. The derivation of dispersion relation for the pipes coupled with DVA is not straightforward, therefore numerical model is used in these situations. The optimal stiffness-damping values of DVA are calculated by genetic algorithm (GA) optimization given in Section 2.3.

2.1. Dispersion equation

For the analysis of flexural wave propagation in the pipe system shown in Fig. 1, a typical unit-cell of pipe with span *L* shown in Fig. 3 is used. The transfer matrix method (TMM) and Floquet–Bloch periodic condition is employed to formulate the dispersion equation. The Floquet–Bloch theorem relates the displacements at the boundary DoFs of adjacent unit-cells. The left and right ends of the pipe are represented by x_r and x_{r+1}, respectively.

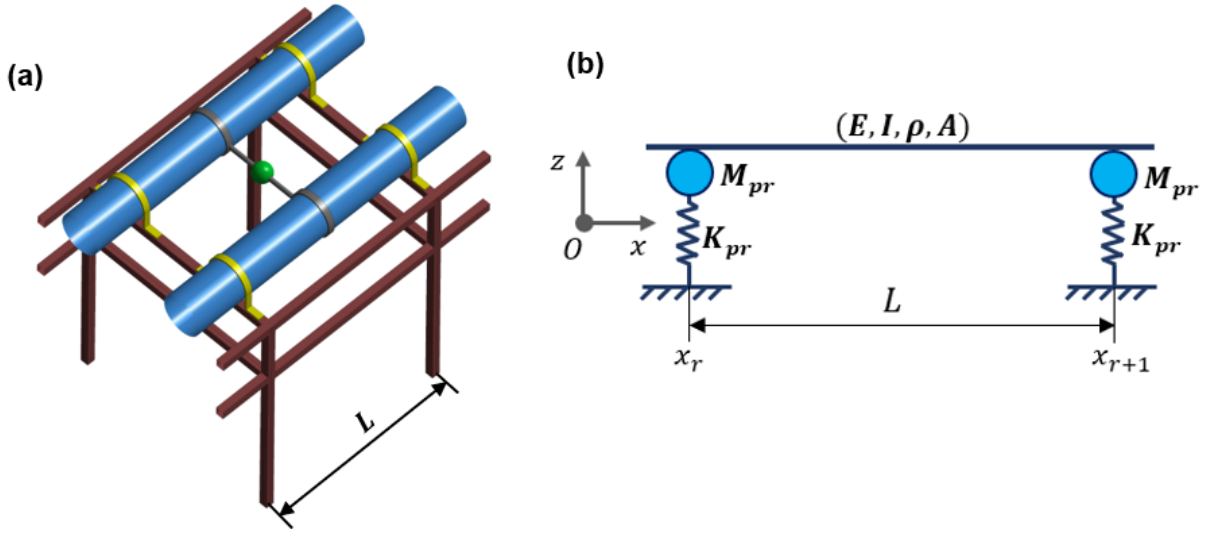

Fig. 3. Schematics of a unit-cell shown in Fig. 1: (a) Representation of r^{th} span; and (b) Simplified model showing a single span of pipe P_1.

The pipe is assumed to be undamped and modelled as a Euler-Bernoulli beam. The transverse displacement $z(x,t)$ of the pipe at position x and time t is given by the following differential equation:

$$\frac{\partial^2}{\partial x^2}\left[EI\frac{\partial^2 z(x,t)}{\partial x^2}\right] + \rho A\frac{\partial^2 z(x,t)}{\partial t^2} = 0 \tag{1}$$

where E, I, ρ, and A denote the Young's modulus, moment of inertia, density and cross-sectional area, respectively. A harmonic solution of Eq. (1) can be assumed as,

$$z(x,t) = Z(x,\omega)e^{\mathrm{i}\omega t} \tag{2}$$

where $Z(x,\omega)$ and $\omega = 2\pi f$ represent the frequency dependent amplitude, and frequency of the wave, respectively, and $\mathrm{i} = \sqrt{-1}$. Substitution of Eq. (2) in Eq. (1) gives,

$$EI\frac{\partial^4 Z(x,\omega)}{\partial x^4} - \rho A\omega^2 Z(x,\omega) = 0 \tag{3}$$

The solution of (3) in frequency domain is expressed as,

$$Z(x,\omega) = A_1 e^{\beta x} + A_2 e^{-\beta x} + A_3 e^{\mathrm{i}\beta x} + A_4 e^{-\mathrm{i}\beta x} \tag{4}$$

where A_1, A_2, A_3 and A_4 are the wave mode coefficients that depend on ω, and $\beta = \left(\frac{\rho A\omega^2}{EI}\right)^{\frac{1}{4}}$ is the wavenumber.

Rotational angle (θ) is obtained by differentiating $Z(x,\omega)$ with respect to the spatial coordinate x as,

$$\theta(x,\omega) = \frac{\partial Z}{\partial x} = \beta\left(A_1 e^{\beta x} - A_2 e^{-\beta x} + \mathrm{i}A_3 e^{\mathrm{i}\beta x} - \mathrm{i}A_4 e^{-\mathrm{i}\beta x}\right) \tag{5}$$

Bending moment (M) and shear force (V) can be obtained by,

$$M(x,\omega) = -EI\frac{\partial^2 Z}{\partial x^2} \tag{6}$$

$$V(x,\omega) = -EI\frac{\partial^3 Z}{\partial x^3} \tag{7}$$

State vector $\boldsymbol{\psi}(\mathbf{x},\boldsymbol{\omega})$ of the beam consisting of displacement states (transverse displacement $Z(x,\omega)$ and rotation $\theta(x,\omega)$) and force states (bending moment $M(x,\omega)$ and shear force $V(x,\omega)$) is defined as,

$$\boldsymbol{\psi}(\mathbf{x},\boldsymbol{\omega}) = \{Z(x,\omega), \theta(x,\omega), M(x,\omega), V(x,\omega)\}^T$$

The state vector at the left support x_r is,

$$\boldsymbol{\psi}(\mathbf{x_r}) = \begin{Bmatrix} Z(x_r) \\ \theta(x_r) \\ M(x_r) \\ V(x_r) \end{Bmatrix} = \mathbf{T_b}(\mathbf{x_r})\mathbf{A} \tag{8}$$

where $\mathbf{T_b}(\mathbf{x_r}) = \begin{bmatrix} e^{\beta x_r} & e^{-\beta x_r} & e^{\mathrm{i}\beta x_r} & e^{-\mathrm{i}\beta x_r} \\ \beta e^{\beta x_r} & -\beta e^{-\beta x_r} & \mathrm{i}\beta e^{\mathrm{i}\beta x_r} & -\mathrm{i}\beta e^{-\mathrm{i}\beta x_r} \\ -EI\beta^2 e^{\beta x_r} & -EI\beta^2 e^{-\beta x_r} & EI\beta^2 e^{\mathrm{i}\beta x_r} & EI\,\beta^2 e^{-\mathrm{i}\beta x_r} \\ -EI\beta^3 e^{\beta x_r} & EI\beta^3 e^{-\beta x_r} & \mathrm{i}EI\,\beta^3 e^{\beta x_r} & -\mathrm{i}EI\,\beta^3 e^{-\beta x_r} \end{bmatrix}$, and $\mathbf{A} = \{\mathbf{A_1}, \mathbf{A_2}, \mathbf{A_3}, \mathbf{A_4}\}^{\mathbf{T}}$.

The state vector at the right support is obtained by replacing x_r with x_{r+1} in Eq. (8), resulting in,

$$\boldsymbol{\Psi}(\mathbf{x_{r+1}}) = \mathbf{T_b}(\mathbf{x_{r+1}})\mathbf{A} \tag{9}$$

Eq. (9) can be rewritten as,

$$\boldsymbol{\Psi}(\mathbf{x_{r+1}}) = \mathbf{T_{tb}}\boldsymbol{\psi}(\mathbf{x_r}) \tag{10}$$

where $\mathbf{T_{tb}} = \mathbf{T_b}(\mathbf{x_{r+1}})\ \mathbf{T_b}^{-1}(\mathbf{x_r})$ represents transfer matrix of beam, and can be expressed as,

$$\mathbf{T_{tb}} = \begin{bmatrix} (\Phi_1 + \Phi_2) & \dfrac{(\Phi_3 + \Phi_4)}{\beta} & \dfrac{(\Phi_1 - \Phi_2)}{\beta^2 EI} & \dfrac{(\Phi_3 - \Phi_4)}{\beta^3 EI} \\ -\beta(\Phi_3 - \Phi_4) & (\Phi_1 + \Phi_2) & -\dfrac{(\Phi_3 + \Phi_4)}{\beta EI} & \dfrac{(\Phi_1 - \Phi_2)}{\beta^2 EI} \\ \beta^2 EI(\Phi_1 - \Phi_2) & \beta EI(\Phi_3 - \Phi_4) & (\Phi_1 + \Phi_2) & \dfrac{(\Phi_3 + \Phi_4)}{\beta} \\ -\beta^3 EI(\Phi_3 + \Phi_4) & \beta^2 EI(\Phi_1 - \Phi_2) & -\beta(\Phi_3 - \Phi_4) & (\Phi_1 + \Phi_2) \end{bmatrix} \tag{11}$$

where $\Phi_1 = \cos(\beta L)/2$, $\Phi_2 = \cosh(\beta L)/2$, $\Phi_3 = \sin(\beta L)/2$ and $\Phi_4 = \sinh(\beta L)/2$.

Similarly, transfer matrix characterizing wave propagation through the rack which is idealized as a SDoF system with a lumped mass M_{pr} and stiffness K_{pr} is denoted as $\mathbf{T_{pr}}$, and is given by,

$$\mathbf{T_{pr}} = \begin{bmatrix} 1 & 0 & 0 & 0 \\ 0 & 1 & 0 & 0 \\ 0 & 0 & 1 & 0 \\ K_{pr} - M_{pr}\omega^2 & 0 & 0 & 1 \end{bmatrix} \tag{12}$$

Incorporating $\mathbf{T_{pr}}$ in Eq. (10), cumulative transfer matrix $\mathbf{T}$ of coupled pipe-rack structure will be,

$$\mathbf{\Psi(x_{r+1})} = \mathbf{T_{pr}T_{tb}\Psi(x_r)} = \mathbf{T\Psi(x_r)} \tag{13}$$

Owing to the periodicity in x direction, the state vectors at the ends r and $r+1$ are related using the Floquet-Bloch's theorem [73,74] as,

$$\mathbf{\Psi(x_{r+1})} = e^{-i\kappa L}\mathbf{\Psi(x_r)} \tag{14}$$

Here, κ is wavenumber of the flexural wave propagating in the coupled pipe-rack structure. Substituting Eq. (14) in (13) yields a standard eigenvalue problem as,

$$\left[\mathbf{T} - e^{-i\kappa L}\mathbf{I_4}\right]\mathbf{\Psi(x_r)} = \mathbf{0} \tag{15}$$

where $\mathbf{I_4}$ is 4×4 identity matrix. For existence of a non-trivial solution for (15), the determinant of $\left[\mathbf{T} - e^{-\mathrm{i}\kappa L}\mathbf{I_4}\right]$ should be zero. Thus,

$$\left|\mathbf{T} - e^{-\mathrm{i}\kappa L}\mathbf{I_4}\right| = \mathbf{0} \tag{16}$$

The solution of (16) represents the relation between κ and ω, and indicates the dispersion equation for the coupled pipe-rack system shown in Fig. 2 (a). It is given as,

$$\begin{aligned}
&[\{\Phi_2 - \Phi_1\}^2 - \{\Phi_4^2 - \Phi_3^2\}]\cos^2(\kappa L) \\
&\quad + 2\Bigg[\{\Phi_4 - \Phi_3\}\{\Phi_2\,\Phi_3 + \Phi_1\Phi_4\} - \{\Phi_2\,\Phi_3 - \Phi_1\Phi_4\}\{\Phi_3 + \Phi_4\} \\
&\quad + \frac{\{\Phi_4 - \Phi_3\}\{1 - \Phi_1\Phi_2\}\{K_{pr} - M_{pr}\omega^2\}}{8EI\beta^3}\Bigg]\cos(\kappa L) \\
&\quad + \Bigg[4\{\Phi_3^2\Phi_2^2 - \Phi_1^2\Phi_4^2\} - \{\Phi_2 - \Phi_1\}^2 \\
&\quad + \frac{\{\Phi_2\Phi_3 - \Phi_1\,\Phi_4\}\{1 - \Phi_1\Phi_2\}\{K_{pr} - M_{pr}\omega^2\}}{2EI\beta^3}\Bigg] = 0
\end{aligned} \tag{17}$$

Coefficients Φ_1, Φ_2, Φ_3 and Φ_4 in Eq. (17) are function of β, the solution of which yields two pairs of wave number $\pm\kappa_1$ and $\pm\kappa_2$ for each ω. Here, each pair represents identical waves traveling in opposite direction. In general, κ may be real, purely imaginary, or complex. If κ is real, the wave passes through each unit-cell without any attenuation, but with a phase change at each unit-cell. Conversely, if κ is purely imaginary, the wave attenuates across each unit-cell vibrating in phase or out of phase, and is referred to as attenuating or evanescent wave. For a complex κ, waves of certain frequency propagate while others get attenuated, resulting in the presence of both PBs and BGs in the dispersion diagram [75].

2.2. Numerical Modelling

To validate the analytical dispersion relations calculated using Eq. (17), a FE model of P_1 coupled to rack as shown in Fig. 2(a) is built for forty spans using ANSYS APDL [76]. The pipe is modelled using BEAM4 element which is a 2-node Euler-Bernoulli beam, while for the spring and lumped mass, COMBIN14 and MASS21 elements are respectively used.

Let $\mathbf{M} \in \mathbb{R}^{n\,x\,n}$, $\mathbf{K} \in \mathbb{R}^{n\,x\,n}$ and $\mathbf{C} \in \mathbb{R}^{n\,x\,n}$ respectively be the mass, stiffness and damping matrices of the coupled pipe-rack system which has n DoFs. If $\{\ddot{\boldsymbol{q}}\} \in \mathbb{R}^{n\,x\,1}$, $\{\dot{\boldsymbol{q}}\} \in \mathbb{R}^{n\,x\,1}$ and $\{\boldsymbol{q}\} \in \mathbb{R}^{n\,x\,1}$ respectively denote the acceleration, velocity, and displacement at time t, the system's equation of motion without any external excitation is given by,

$$\mathbf{M}\{\ddot{\mathbf{q}}\} + \mathbf{C}\{\dot{\mathbf{q}}\} + \mathbf{K}\{\mathbf{q}\} = \{\mathbf{0}\} \tag{18}$$

If the displacement is given at g DoFs, Eq. (18) can be rewritten as,

$$\begin{bmatrix}\mathbf{M_{hh}} & \mathbf{M_{hg}}\\ \mathbf{M_{gh}} & \mathbf{M_{gg}}\end{bmatrix}\begin{Bmatrix}\ddot{\mathbf{q}}_\mathbf{h}\\ \ddot{\mathbf{q}}_\mathbf{g}\end{Bmatrix} + \begin{bmatrix}\mathbf{C_{hh}} & \mathbf{C_{hg}}\\ \mathbf{C_{gh}} & \mathbf{C_{gg}}\end{bmatrix}\begin{Bmatrix}\dot{\mathbf{q}}_\mathbf{h}\\ \dot{\mathbf{q}}_\mathbf{g}\end{Bmatrix} + \begin{bmatrix}\mathbf{K_{hh}} & \mathbf{K_{hg}}\\ \mathbf{K_{gh}} & \mathbf{K_{gg}}\end{bmatrix}\begin{Bmatrix}\mathbf{q}_\mathbf{h}\\ \mathbf{q}_\mathbf{g}\end{Bmatrix} = \begin{Bmatrix}\mathbf{0}_\mathbf{h}\\ \mathbf{0}_\mathbf{g}\end{Bmatrix} \tag{19}$$

where, h refers the DoFs other than the g DoFs ($g + h = n$). First row in (19) gives,

$$\mathbf{M_{hh}}\{\ddot{\mathbf{q}}_\mathbf{h}\} + \mathbf{C_{hh}}\{\dot{\mathbf{q}}_\mathbf{h}\} + \mathbf{K_{hh}}\{\mathbf{q}_\mathbf{h}\} = -\left(\mathbf{M_{hg}}\{\ddot{\mathbf{q}}_\mathbf{g}\} + \mathbf{C_{hg}}\{\dot{\mathbf{q}}_\mathbf{g}\} + \mathbf{K_{hg}}\{\mathbf{q}_\mathbf{g}\}\right) \tag{20}$$

To determine the steady state response at h DoFs under a given displacement $\{\mathbf{q}_\mathbf{g}\} = \{\mathbf{\Omega}_\mathbf{g}\}e^{\mathrm{i}\omega t}$, a solution to $\{\mathbf{q}_\mathbf{h}\}$ of the form $\{\mathbf{q}_\mathbf{h}\} = \{\mathbf{\Omega}_\mathbf{h}\}e^{\mathrm{i}\omega t}$ is assumed, substitution of which in (20) leads to,

$$\{\mathbf{\Omega}_\mathbf{h}\} = -[-\omega^2\mathbf{M_{hh}} + \mathrm{i}\omega\mathbf{C_{hh}} + \mathbf{K_{hh}}]^{-1}\left[-\omega^2\mathbf{M_{hg}} + \mathrm{i}\omega\mathbf{C_{hg}} + \mathbf{K_{hg}}\right]\{\mathbf{\Omega}_\mathbf{g}\} \tag{21}$$

The pipe-rack system considered in this study is periodic along the length of pipe. Various techniques can be employed to induce flexural vibration in the piping system. Here, to mobilize the periodicity and replicate the flexural vibration in P_1, a harmonic rotation $\Omega_g e^{\mathrm{i}2\pi ft}$ with unit amplitude is imposed at the left end of the pipe. The resulting steady-state output rotation $\Omega_h(f)$ is then computed at the right end. The vibration transmission T_r (dB) behavior in the piping system can be described by,

$$T_r(f) = 20\ log_{10}\left|\frac{\Omega_h(f)}{\Omega_g(f)}\right| \tag{22}$$

The frequency ranges where T_r falls below zero denote BGs. To ensure their accuracy, the variation of T_r is compared with the dispersion relations obtained from Eq. (17).

2.3. Vibration control method

DVA is employed for controlling vibrations in a particular PB in the pipelines. For an efficient control with a given mass ratio μ ($\mu = m_\mu/(\rho Al)_{P_1}$, where m_μ is mass of the DVA), optimal values of springs ($k_{1,\mu}$ and $k_{2,\mu}$) and dampers ($c_{1,\mu}$ and $c_{2,\mu}$) have to be employed. Let $\|H_{Uncontrol}\|_\infty$ and $\|H_{control}\|_\infty$ represent the peak value of T_r calculated over the frequencies of interest without and with DVAs, respectively. The efficiency of DVA is quantified using a performance metric Π as,

$$\Pi = \|H_{Control}\|_\infty / \|H_{Uncontrol}\|_\infty \tag{23}$$

A lower value of Π indicates better performance of DVA and vice-versa. Thus, for a specified μ, optimal properties of DVA are those that minimize the metric Π. Although multiple techniques are available for numerically evaluating these optimal properties [77], the widely used GA technique [66,67] is adopted here, and is explained in the following section.

2.3.1. GA optimization scheme

Optimization for the design of DVA shown in Fig. 2(b) is formulated as,

$$\begin{Bmatrix} k_{1,\mu} \\ k_{2,\mu} \\ c_{1,\mu} \\ c_{2,\mu} \end{Bmatrix} = \arg\min(\Pi) \tag{24}$$

subjected to,

$$\{\mathbf{LB}\} \leq \begin{Bmatrix} k_{1,\mu} \\ k_{2,\mu} \\ c_{1,\mu} \\ c_{2,\mu} \end{Bmatrix} \leq \{\mathbf{UB}\} \tag{25}$$

where $\{\mathbf{LB}\} \in \mathbb{R}^{4\,x\,1}$ and $\{\mathbf{UB}\} \in \mathbb{R}^{4\,x\,1}$ denote the lower and upper bound for the design variables, respectively. These bounds are set to ensure that the design variables remain in realistic range, facilitating faster optimization. Similarly, the optimal parameters (k_μ and c_μ) for the conventional TMD are determined. The value of Π is computed over a frequency range within the passband to be controlled.

GA is a stochastic search method based on the principles of natural selection and genetics [78]. Within the prescribed upper and lower bounds (UB and LB), a random initial generation $\mathbf{X_0} \in \mathbb{R}^{p\,x\,4}$ is created where p is the number of children. The fitness function Π is determined for the current generation by employing the corresponding FE models. New generations are generated according to the values of the current fitness function, progressively evolving towards the optimal solution. From generation j, $j+1$ is obtained through a combination of three methods; selection, crossover and mutation. In selection, s set of solutions in $\mathbf{X_j}$ possessing the best Π values are chosen and included in the $j+1^{th}$ generation as $\mathbf{X_{j,s}} \in \mathbb{R}^{s\,x\,4}$. Crossover produces c new solutions $\mathbf{X_{j,c}} \in \mathbb{R}^{c\,x\,4}$ by merging two best solutions from $\mathbf{X_j}$, while mutation applies random changes to solution in $\mathbf{X_j}$ to generate m children $\mathbf{X_{j,m}} \in \mathbb{R}^{m\,x\,4}$. Selection was performed using tournament technique, while for mutation and crossover a random Gaussian distribution was employed [79]. The diversity of the subsequent generation $j+1$ depends on the proportion of children from selection, crossover, and mutation ($s:c:m$). The new generation $\mathbf{X_{j+1}} \in \mathbb{R}^{p\,x\,4}$ comprising children from selection, crossover and mutation ($\mathbf{X_{j+1}} = \mathbf{X_{j,s}} \cup \mathbf{X_{j,c}} \cup \mathbf{X_{j,m}}$ and $p = s + c + m$), is now employed to determine Π as before. This iterative process is continued till the required convergence criterion is achieved. Fig. 4 demonstrates this algorithm.

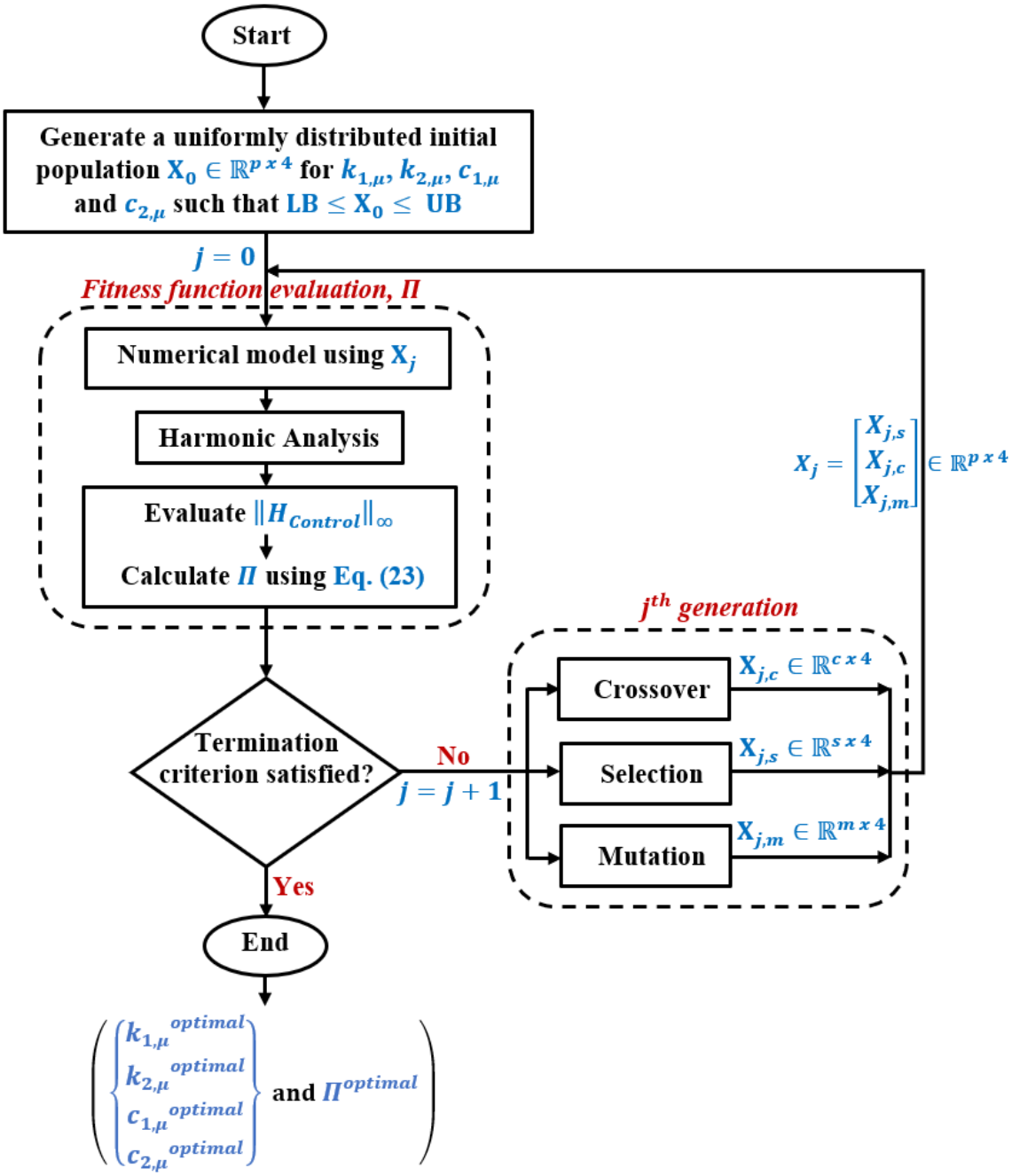

Fig. 4. Flow-chart for GA optimization process for the design of DVA with mass ratio μ.

3. Results and discussions

The dispersion characteristics of flexural wave are initially explored in the coupled pipe-rack system, along with an extreme scenario of pipe with simple supports (where the rack stiffness K_{pr}

tends to infinity and the lumped mass M_{pr} approaches zero). FE models are employed to verify the resulting BG properties obtained from analytical models. Subsequently, DVA with different mass ratio (μ) is designed to control vibrations in a specific PB. Finally, the efficacy of the designed DVA is estimated by employing a white Gaussian noise as input excitation.

3.1. Dispersion diagram

The dispersion relationship in Eq. (17) is used to obtain the flexural BG properties. Figures 5(a) and (b) respectively show the frequency-dependent variations of the real and imaginary parts of both positive and negative wavenumbers ($\pm\kappa_1 L$). It can be noticed that both the waves exhibit identical attenuation and propagation behaviors, but of opposite nature. The BGs are observed at $0-4.50$ Hz, $5.50-31.10$ Hz and $71.10-124.40$ Hz, and are depicted by shaded areas. Figure 5(c) shows T_r from FE model calculated based on Eq. (22). The similarity in terms of position and width of BG between analytical and FE results confirms the reliability of the developed models. A non-zero value of $\mathrm{Im}(\pm\kappa_1 L)$ indicates the BG regions, where no waves propagate in the piping system. In contrast, PBs are the frequency ranges where $\mathrm{Im}(\pm\kappa_1 L)$ is zero, allowing waves to propagate freely through the system. The first BG in this system stems from the LR of the rack structure, and its position is governed by the stiffness and mass properties associated with the rack's geometry. However, the other BGs arise from the BS phenomenon associated with spatial periodicity, which in this case depends on the distance between two successive columns of the rack.

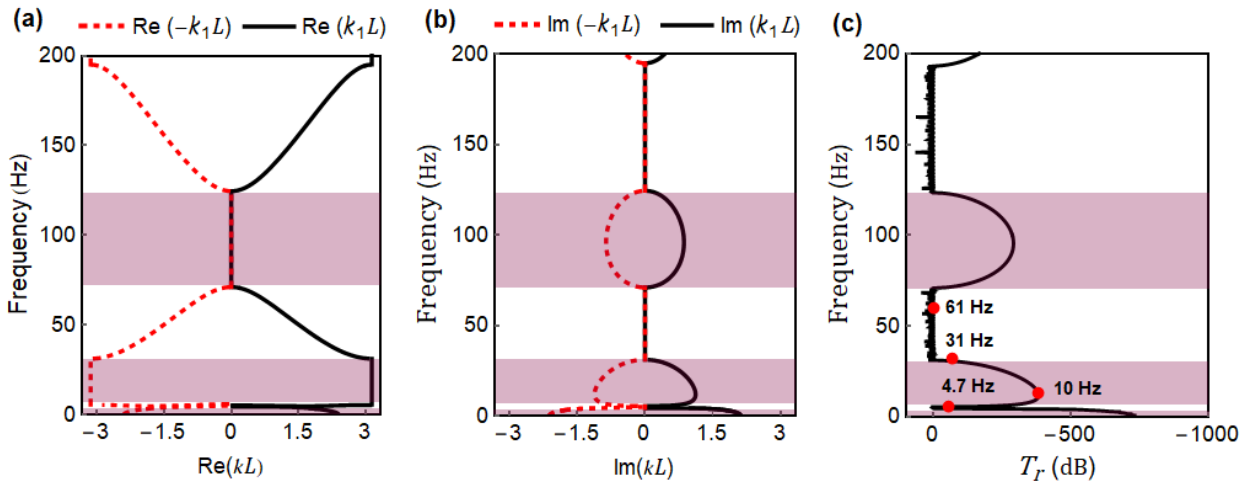

Fig. 5. Dispersion diagram and vibration transmission in P_1 with rack: (a) $\mathrm{Re}(\pm\kappa_1 L)$; (b) $\mathrm{Im}(\pm\kappa_1 L)$; and (c) T_r (dB).

To better understand the propagation behavior of waves in the coupled pipe-rack system, four typical frequencies (4.7 Hz, 10 Hz, 31 Hz, and 61 Hz) as indicated in Fig. 5 (c) are selected. The first and last frequencies fall within the PBs caused by rack and pipe, respectively, while the remaining two lie in BGs. The resulting steady state displacement profiles in z direction (from $\begin{Bmatrix}\Omega_h\\ \Omega_g\end{Bmatrix}$) at these frequencies are depicted in Fig. 6. The frequency of 4.7 Hz fall in PB, this wave passes through the structure with considerable amplitude, which can be seen in Fig. 6(a). Conversely, the attenuation at 10 Hz is remarkably high, as evidenced by the rapidly diminishing displacement along the pipe depicted in Fig. 6(b). Similarly, the displacement plot at 31 Hz shown in Fig. 6(c) indicates the attenuation in the BG. However, its amplitude does not decay as rapidly as compared to that at 10 Hz. Unlike the displacement profiles at BGs, no attenuation is observed at 61 Hz. Figure 6(d) confirms this. A comparison of the displacement profile at 4.7 Hz and 61 Hz shows the difference in the type of PB. The one at 4.7 Hz is from LR of the rack, while first bending mode of the pipe resulted in the PB around 61 Hz.

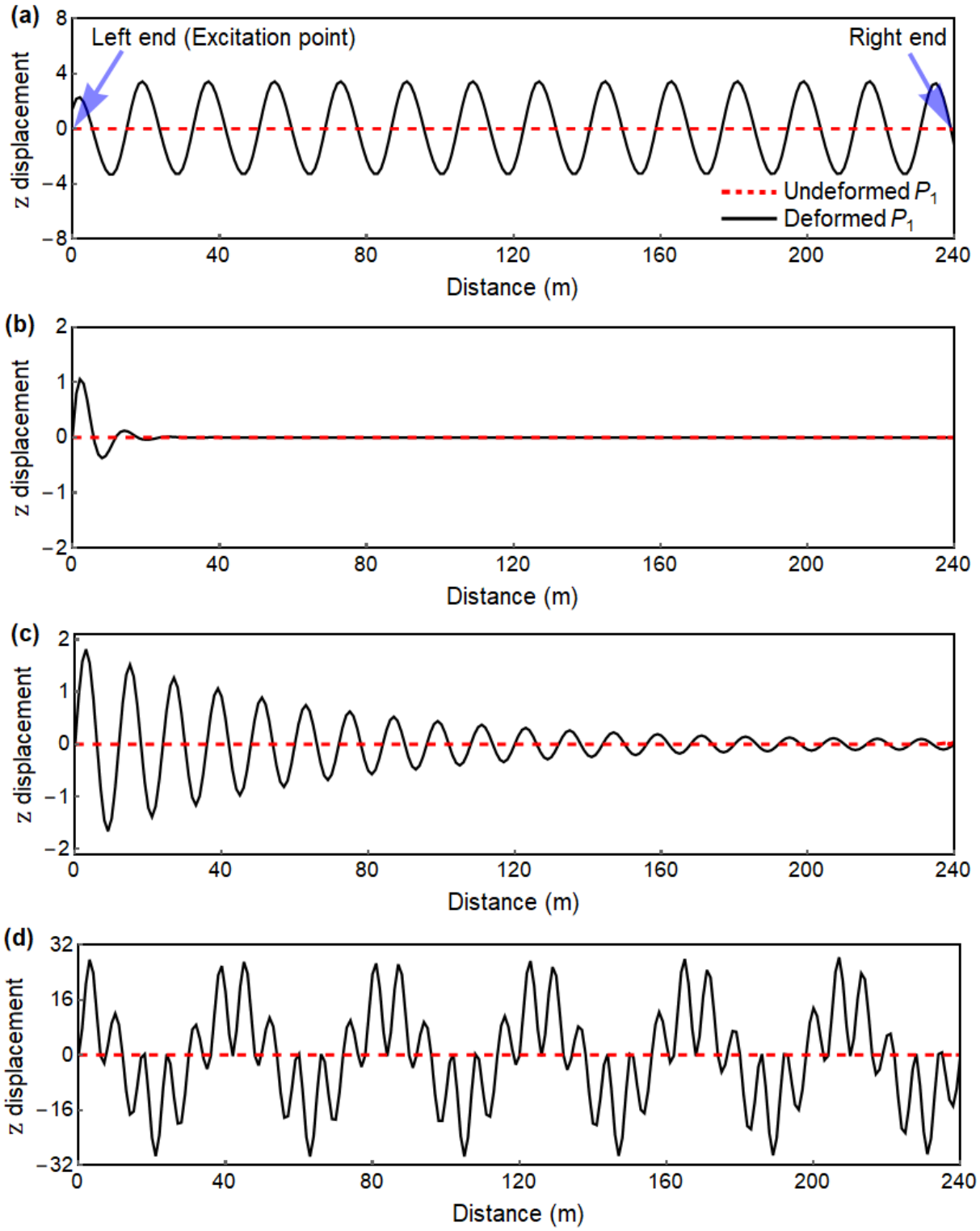

Fig. 6. Steady-state displacement profiles of P_1 at different excitation frequencies indicated in Fig. 5(c): (a) 4.7 Hz; (b) 10 Hz; (c) 31 Hz; and (d) 61 Hz.

PBs in a periodic structure align with the cluster of corresponding natural frequencies [80]. The clustering of natural frequencies in PBs and the attenuation strength within BGs depend on the number of unit-cells N_u. To illustrate this, the variation of natural frequencies corresponding to N_u= 5, 10, 20, 30 and 40 is shown in Fig. 7. The BGs are depicted by shaded regions. As can be seen, bounding frequencies of PBs are not same for different values of N_u. As N_u increases, the bounding frequencies become closer to the analytically predicted PB frequencies. It is noted that the number of eigenfrequencies within each PB increases with increase in N_u. Let f_s^{FE} and f_t^{FE} respectively represent the starting and terminal frequencies of PBs calculated from FE model, and f_s^{AN} and f_t^{AN} represent the corresponding values from analytical dispersion relation which is independent of N_u. The percentage difference in the starting frequencies of PBs from analytical and FE model for a given N_u is calculated as [19],

$$\Delta_s = \frac{f_s^{AN} - f_s^{FE}}{f_s^{FE}} * 100 \tag{26}$$

Identical relations can be used to obtain the percentage difference Δ_t in terminal frequencies. The values of Δ_s and Δ_t corresponding to various PBs for different values of N_u are reported in Table 1. A small reduction is found in Δ_s for first PB as N_u increases from 5 to 10, and become constant with further increase in N_u. On the other hand, a very small increase in Δ_s occurs for the other two PBs with an increase in N_u until 30. A significant drop in Δ_t is noted for all PBs as N_u increases from 5 to 10, with only a slight reduction noted for other values. However, no change in Δ_s and Δ_t is observed for N_u= 30 and 40. Based on Fig. 7 and Table 1, it can be summarized that a finite structure needs to have an adequate N_u to accurately replicate the attenuation and propagation behavior of the corresponding infinite periodic structure.

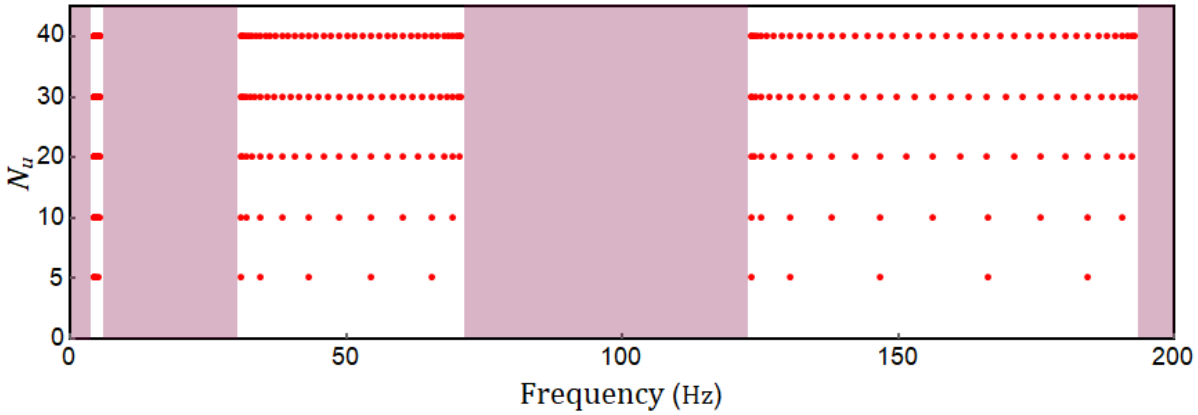

Fig. 7. Comparison of eigenfrequencies of P_1 on rack for different values of N_u.

Table 1

Percentage difference in analytical and numerically determined PB bounding frequencies for P_1.

N_u	Ist PB		IInd PB		IIIrd PB	
	Δ_s (%)	Δ_t (%)	Δ_s (%)	Δ_t (%)	Δ_s (%)	Δ_t (%)
5	0.29	5.32	0.03	8.36	0.89	5.71
10	0.17	1.45	0.07	2.34	0.91	2.23
20	0.17	0.28	0.09	0.76	0.91	1.29
30	0.17	0.02	0.10	0.36	0.91	1.10
40	0.17	0.02	0.10	0.36	0.91	1.10

Figure 8(a) shows the variation of T_r at four typical points along the length of pipe; 24 m, 84 m, 144 m, and 240 m from the excitation point. This corresponds to the right end of 4th, 14th, 24th and 40th span of P_1. It is evident that the attenuation level within each BG increases significantly when moving away from the excitation point, reaching its maximum at 240 m. However, the number of BGs and their positions is independent of the locations. Figure 8(b) depicts the comparison of T_r

when 4, 14, 24 and 40 unit-cells are used in the FE model. Within each PB, the transmission peaks are notably high and they remain consistent even for the smallest distance, while the number of peaks varies with N_u.

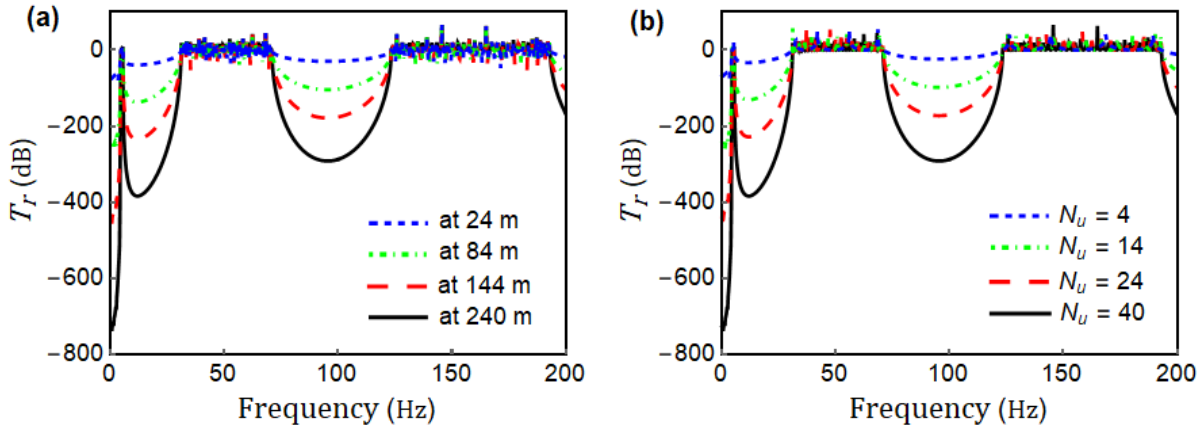

Fig. 8. Comparison of T_r for P_1: (a) At different location from excitation point; and (b) For different values of N_u.

As the stiffness of the rack become extremely high ($K_{pr} \to \infty$) and the lumped mass become negligible ($M_{pr} = 0$), coupled pipe-rack system reduces to a pipe supported on simple supports. Substituting these conditions in Eq. (17) results in the following dispersion equation,

$$\cos(\kappa L) = 2\left[\frac{\Phi_2\Phi_3 - \Phi_1\Phi_4}{\Phi_3 - \Phi_4}\right] \tag{27}$$

Figures 9(a) and (b) respectively illustrates the $\mathrm{Re}(\pm\kappa_1 L)$ and $\mathrm{Im}(\pm\kappa_1 L)$ parts of the dispersion relation based on Eq. (27), while Fig. 9(c) illustrates the variation of T_r from FE model. The analytical and FE results exhibit good agreement with each other. The first two BGs are observed at $0 - 31.10$ Hz and $71.30 - 123.30$ Hz. The principal difference in the dispersion characteristic between the case with and without rack lie in the existence of an extra narrow PB located around

4.50 Hz in case of the former. The pipe supported on rack exhibits both resonance and Bragg-type BGs, whereas only Bragg BGs appear with simple supports.

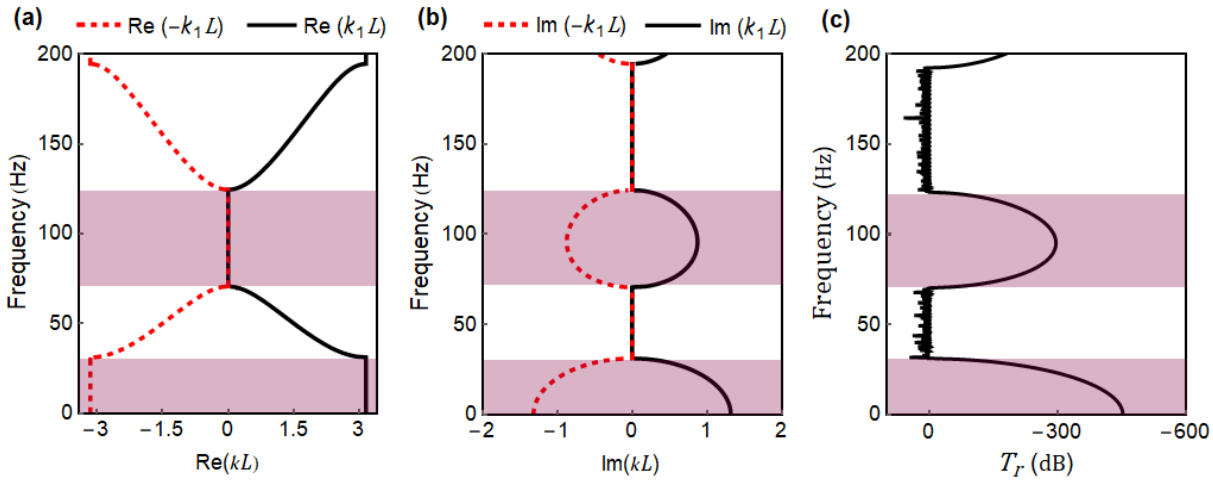

Fig. 9. Dispersion diagram and vibration transmission in pipe P_1 with simple supports: (a) $\mathrm{Re}(\pm\kappa_1 L)$; (b) $\mathrm{Im}(\pm\kappa_1 L)$; and (c) T_r (dB).

3.2. Vibration control in dual pipelines

The propagation and attenuation characteristics of uncontrolled P_1 coupled with rack discussed in the previous section shows the presence of wide PBs in the low frequency region. Herein, it is aimed to control second PB ($31.10 - 71.10$ Hz). To achieve this, a SDoF DVA is connected with the pipes P_1 and P_2 as illustrated in Fig. 2(b). For any value of μ, the optimal stiffness ($k_{1,\mu}$, $k_{2,\mu}$) and damping ($c_{1,\mu}$, $c_{2,\mu}$) properties to be employed in the DVA are determined using GA given in Section 2.3. The optimal parameters for DVA and the corresponding Π values are obtained for three mass ratios (μ = 10%, 15% and 20%), and given in Table 2.

Figures 10(a) and (b) compare the T_r from uncontrolled P_1 and P_2 against controlled cases using DVA for the three mass ratios. It can be observed from both Table 2 and Fig. 10 that the performance of DVAs in the considered PB improves with an increase in μ. A small value of Π indicates high vibration reduction capabilities in the controlled system and vice versa.

Table 2

Optimal properties of DVA.

Mass ratio (%)	Stiffness (N/m)		Damping (N − s/m)		Objective function
μ	$k_{1,\mu}$	$k_{2,\mu}$	$c_{1,\mu}$	$c_{2,\mu}$	Π
10	2.87E6	6.53E3	4.98E3	3.77E2	6.59E-4
15	4.23E6	5.31E4	1.38E4	4.38E2	2.49E-4
20	4.14E6	1.07E6	7.24E3	8.77 E3	4.09E-5

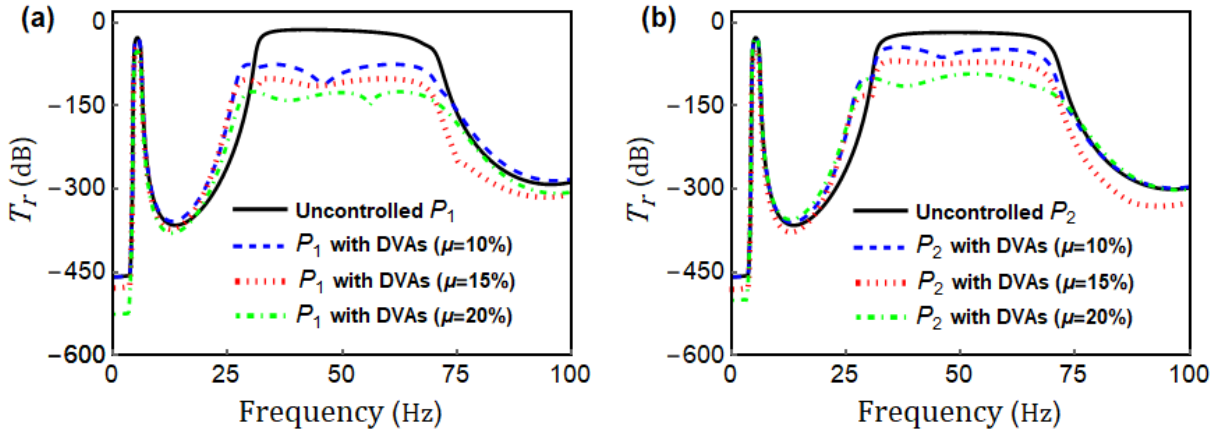

Fig. 10. Comparison of T_r in uncontrolled pipe against pipe controlled using DVAs with different μ: (a) P_1; (b) P_2.

3.3 *Efficacy of designed DVA*

To assess the effectiveness of the designed DVA, its performance is compared to that of the pipe endowed with conventional TMD of the same mass ratio. The optimal values of k_μ and c_μ in case of TMD with μ = 10% are obtained using optimization as 1.16 E6 N/m and 7.40E3 N − s/m, respectively. The corresponding Π is 4.98E-5. Figure 11 compares the T_r of uncontrolled P_1 against P_1 with DVAs and TMDs. As evident from Fig. 11 and the value of Π, the performance of

TMD is slightly better than the DVA. However, the principal advantage of the DVA is that a single mass can simultaneously control the two pipes, while a conventional TMD with a single mass can control only that pipe to which it is attached.

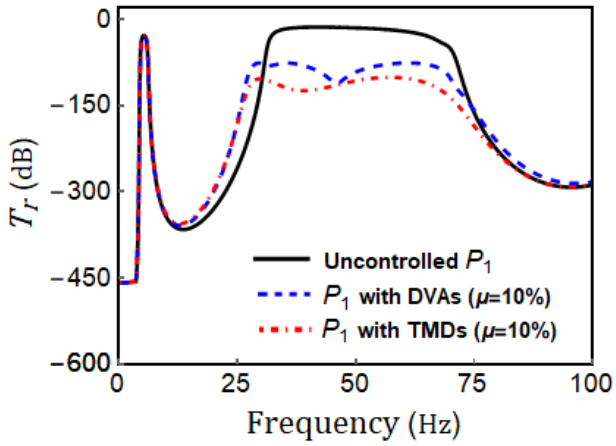

Fig. 11. Comparison of T_r in uncontrolled P_1 against P_1 controlled using DVAs and conventional TMDs for $\mu = 10\%$.

Further, to test the effectiveness of the designed DVAs, a random white Gaussian noise (with zero-mean and unit standard deviation) rotation $RY_{i/p}$ is imposed at the left end of P_1, and the resulting output $RY_{o/p}$ is computed at the right end. $RY_{i/p}$ is generated over a duration of 3 s with a step of $2\text{E} - 3$ s. This results in flexural waves to propagate through the pipe, thereby showcasing its band gap characteristics. Similar flexural wave propagation at different frequencies happens when units such as compressors and pumps are connected to either end of the pipe or from impacts. This is different from seismic or wind loads which follow a different mechanism. A specific realization of $RY_{i/p}$ employed here is shown in Fig. 12(a), and its Fast Fourier Transform (FFT) is depicted in Fig. 12(b).

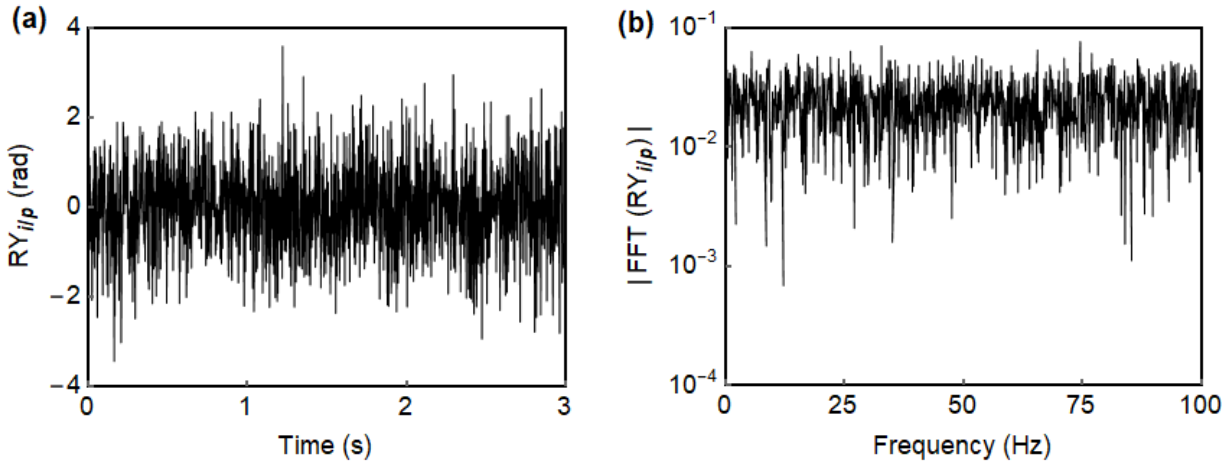

Fig.12. $RY_{i/p}$ imposed at P_1: (a) Time history; and (b) FFT.

A dynamic time history analysis was performed using Newmark-β method with integration parameters $\gamma = 1/2$ and $\eta = 1/6$ [81]. Rayleigh damping was applied only to the pipe-rack system and not for DVA. A damping ratio of $\xi = 2\%$ was considered, and the damping coefficients ($\mathbf{C} = \alpha\mathbf{M} + \delta\mathbf{K}$) for both stiffness and mass were calculated based on a frequency range of $0 - 71.10$ Hz. The analysis is reported only for the case of $\mu = 10\%$, as other cases showed similar patterns.

The time history response $RY_{o/p}$ of uncontrolled and controlled pipes are depicted in Figs. 13(a-c), and Fig. 13(d) compares their FFTs. It is evident from the time history plots that the designed DVA can significantly reduce the vibration response of both pipes. The FFTs in Fig. 13(d) also confirm this. It is also clear from the FFT plots that the DVA is efficient only in the designed frequency range, and may not show the intended performance outside this range. Similar time history and FFT responses are observed for pipes with TMDs; hence, they are not reported.

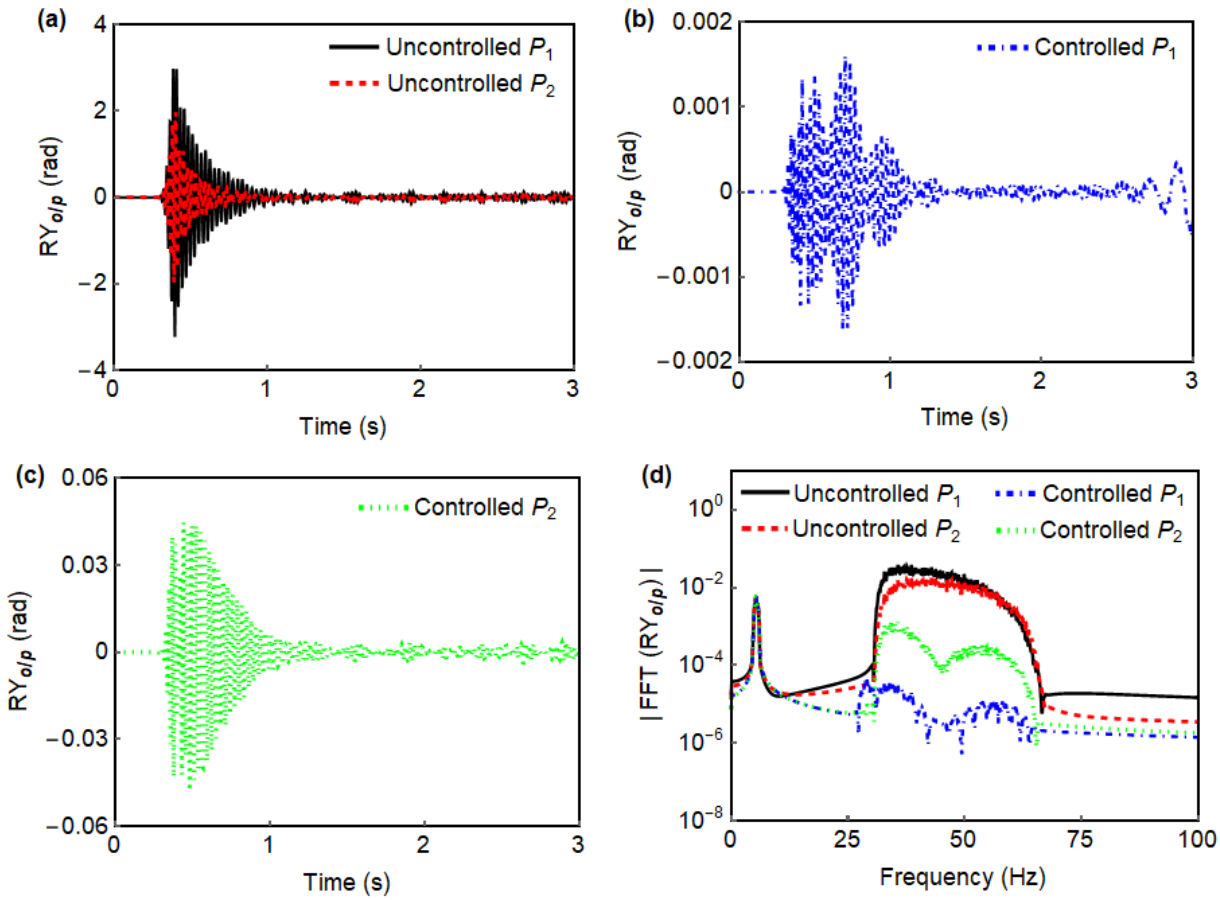

Fig. 13. Response time histories and FFT: (a) Uncontrolled P_1 and P_2; (b) Controlled P_1; (c) Controlled P_2; and (d) Comparison of uncontrolled and controlled pipes FFTs.

4. Conclusions

The study explored the behavior of flexural waves in pipes for two different scenarios; one with a rack structure and the other featuring simple supports. The dispersion relations for both cases were formulated using the transfer matrix method in combination with the Floquet-Bloch's theorem. The resulting band gaps (BGs) and pass bands (PBs) in the considered frequency range were validated using finite element models. Within the analyzed frequency range, pipe supported on rack-structure displayed resonance and Bragg-type BGs, whereas only Bragg BGs were observed in the pipe with simple supports. The modal analysis revealed that a finite structure requires an

adequate number of unit-cells to accurately replicate the behavior of an infinite periodic structure. It was observed that for a given number of spans, attenuation level within each BG increases with distance along the pipe. A similar enhancement in attenuation level was noted as the number of unit-cells increased.

Further, a novel method to control vibration in dual periodic pipelines was proposed, which involves connecting them with a dynamic vibration absorber (DVA) unit in each span. The optimal properties of DVA for different mass ratios were determined using GA based optimization. The performance of DVA increases with an increase in mass ratio. The proposed DVA effectively control vibration in the targeted PB. The performance of the DVA was also compared with the conventional tuned mass damper (TMD) of identical mass ratio. Although the performance of the TMD was slightly higher than the proposed DVA, the former can control only the pipe to which it is attached. In contrast, the DVA can control both pipes simultaneously. Furthermore, a time history analysis was conducted utilizing a white Gaussian noise on both uncontrolled and controlled cases, which confirmed the effectiveness of the designed DVA within the targeted frequency range.

The dispersion relation of flexural elements studied in the context of pipelines can be extended to other similar periodic structures. The innovative concept of interconnected DVA proposed in this study offers a promising and cost-effective solution applicable in scenarios involving secondary flexural systems parallel to the main flexural structure such as periodic railway tracks, closely spaced bridges, underwater tunnels, etc. Although significant efficiency was noted in controlling a particular PB using such mechanisms, the possibility of simultaneous control of multiple PBs, impact of fluid-structure interaction on BG properties, and the effectiveness of proposed technique under other realistic loading scenarios deserve further attention.

Declaration of Competing Interest

The authors declare that they have no known competing financial interests or personal relationships that could have appeared to influence the work reported in this paper.

Acknowledgments

This work was supported by the LABEX CeLyA, France (ANR-10-LABX-0060) of Université de Lyon, within the program ‘‘Investissements d’Avenir’’ operated by the French National Research Agency (ANR).

References

[1] Yan Y, Chai M. Sealing failure and fretting fatigue behavior of fittings induced by pipeline vibration. Int J Fatigue 2020;136:105602. https://doi.org/10.1016/j.ijfatigue.2020.105602.

[2] Bi K, Hao H (2016) Using pipe-in-pipe systems for subsea pipeline vibration control. Eng Struct 109:75–84. https://doi.org/10.1016/j.engstruct.2015.11.018.

[3] Iqbal M, Kumar A, Jaya MM, Bursi OS. Vibration control of periodically supported pipes employing optimally designed dampers. Int J Mech Sci 2022;234:107684. https://doi.org/10.1016/j.ijmecsci.2022.107684.

[4] Shen H, Wen J, Yu D, et al. Stability of fluid-conveying periodic shells on an elastic foundation with external loads. J Fluids Struct 2014;46:134–148. https://doi.org/10.1016/j.jfluidstructs.2014.01.004.

[5] Wang X, Wang MY. An analysis of flexural wave band gaps of locally resonant beams with continuum beam resonators. Meccanica 2016;51:171–178. https://doi.org/10.1007/s11012-015-0197-x.

[6] Xiao L, Iqbal M, Yu X Quasi-static band gaps in metamaterial pipes with negative stiffness resonators. Int J Mech Sci 2023;261:108668. https://doi.org/10.1016/j.ijmecsci.2023.108668.

[7] Iqbal M, Kumar A, Jaya MM (2023) Analysis of Flexural Vibrations and Control of a Periodic Rail Track System. In: In: Shrikhande, M., Agarwal, P., Kumar PCA (eds) (ed) Proceedings of 17th Symposium on Earthquake Engineering. Springer Singapore, Singapore, pp 245–256.

[8] Iqbal M, Kumar A Flexural waves analysis and enhancement of bandgap properties of a periodic track structure. Proc Inst Mech Eng Part E J Process Mech Eng (2022). https://doi.org/10.1177/09544089221145929.

[9] Iqbal M, Kumar A Flexural Vibration Analysis and Improvement of Wave Filtering Capability of Periodic Pipes. Mech Mach Sci 125 MMS (2023):1049–1058. https://doi.org/10.1007/978-3-031-15758-5_108.

[10] Mead DJ. Vibration Response and Wave Propagation in Periodic Structures. J Eng Ind 1970;93: 783–791.

[11] Gupta GS. Natural flexural waves and the normal modes of periodically supported beams and plates. J Sound Vib 1970;13:89–101.

[12] Singh K, Mallik AK. Wave propagation and vibration response of a periodically supported pipe conveying fluid. J Sound Vib 1977;54:55–66.

[13] Yu D, Wen J, Zhao H, et al. Vibration reduction by using the idea of phononic crystals in a pipe-conveying fluid. J Sound Vib 2008;318:193–205. https://doi.org/10.1016/j.jsv.2008.04.009.

[14] Iqbal M, Jaya MM, Bursi OS, et al. Flexural band gaps and response attenuation of periodic piping systems enhanced with localized and distributed resonators. Sci Rep 2020;10:1–11. https://doi.org/10.1038/s41598-019-56724-0.

[15] Pelat A, Gallot T, Gautier F. On the control of the first Bragg band gap in periodic continuously corrugated beam for flexural vibration. J Sound Vib 2019;446:249–262. https://doi.org/10.1016/j.jsv.2019.01.029.

[16] Ding L, Zhu H, Luo H, Yin T. Flexural wave propagation and localization in periodic jointed tunnels subjected to moving loads. J Vib Control 2016;22:2788–2804. https://doi.org/10.1177/1077546314553318.

[17] Zhao P, Yuan L, Ma T, Wei H. Study on Tunable Band Gap of Flexural Vibration in a Phononic. crystals 2021;11:1–12.

[18] Sorokin S V, Broberg PH, Steffensen MT, Ledet LS. Finite element modal analysis of wave propagation in homogeneous and periodic waveguides. Int J Mech Sci 2022;227:107444. https://doi.org/10.1016/j.ijmecsci.2022.107444.

[19] Carta G, Giaccu GF, Brun M. A phononic band gap model for long bridges. The 'Brabau' bridge case. Eng Struct 2017;140:66–76. https://doi.org/10.1016/j.engstruct.2017.01.064.

[20] Guo W, Nie R, Zhu X, et al. Flexural wave band gaps in periodic bi-directionally orthogonal stiffened plates with holes. Int J Struct Stab Dyn 2022;22:1–22. https://doi.org/10.1142/S0219455422501838.

[21] Iqbal M, Kumar A, Bursi OS (2021) Vibration Control of a Periodic Piping System Employing Metamaterial Concept. 2021 15th Int Congr Artif Mater Nov Wave Phenomena, Metamaterials 2021 167–169. https://doi.org/10.1109/Metamaterials52332.2021.9577113

[22] Cai C, Zhou J, Wang K, et al. Quasi-zero-stiffness metamaterial pipe for low-frequency wave attenuation. Eng Struct 2023;279:115580. https://doi.org/10.1016/j.engstruct.2022.115580.

[23] Li J, Yang P, Li S. Multiple band gaps for efficient wave attenuation by inertial amplification in periodic functionally graded beams. Compos Struct 2021;271:114130. https://doi.org/10.1016/j.compstruct.2021.114130.

[24] Burlon A, Failla G. On the band gap formation in locally-resonant metamaterial thin-walled beams. Eur J Mech / A Solids 2023;97:104798. https://doi.org/10.1016/j.euromechsol.2022.104798.

[25] Chen H, Li XP, Chen YY, Huang GL. Wave propagation and absorption of sandwich beams containing interior dissipative multi-resonators. Ultrasonics 2017;76:99–108. https://doi.org/10.1016/j.ultras.2016.12.014.

[26] Wang Q, Li J, Zhang Y, et al. Bandgap properties in metamaterial sandwich plate with periodically embedded plate-type resonators. Mech Syst Signal Process 2021;151:107375. https://doi.org/10.1016/j.ymssp.2020.107375.

[27] Tang L, Cheng L, Chen K. Complete sub-wavelength flexural wave band gaps in plates with periodic acoustic black holes. J Sound Vib 2021;502:116102. https://doi.org/10.1016/j.jsv.2021.116102.

[28] Li L, Chen T, Wang X, Li B. One-dimensional Bi-stage phononic band gap shaft structure for reducing torsional vibration. Appl Mech Mater 2012;141:54–58. https://doi.org/10.4028/www.scientific.net/AMM.141.54.

[29] Song Y, Wen J, Yu D, Wen X. Analysis and enhancement of torsional vibration stopbands in a periodic shaft system. J Phys D Appl Phys 2013;46:. https://doi.org/10.1088/0022-3727/46/14/145306.

[30] Iqbal M, Kumar A, Murugan Jaya M, Bursi OS. Flexural band gaps and vibration control of a periodic railway track. Sci Rep 2021;11:1–13. https://doi.org/10.1038/s41598-021-97384-3.

[31] Yang C, Kaynardag K, Salamone S. Investigation of wave propagation and attenuation in periodic supported rails using wave finite element method. Acta Mech 2023;235: 1453–1469. https://doi.org/10.1007/s00707-023-03484-8.

[32] Li H, Li Y, Liu X. Double-beam metastructure with inertially amplified resonators for flexural wave attenuation. Eur J Mech / A Solids 2023;97:104794. https://doi.org/10.1016/j.euromechsol.2022.104794.

[33] Zhao C, Zhang K, Zhao P, et al. Bandgap merging and backward wave propagation in inertial amplification metamaterials. Int J Mech Sci 2023;250:108319. https://doi.org/10.1016/j.ijmecsci.2023.108319.

[34] Lee S, Ahn CH, Lee JW. Vibro-acoustic metamaterial for longitudinal vibration suppression in a low frequency range. Int J Mech Sci 2018;144:223–234. https://doi.org/10.1016/j.ijmecsci.2018.05.010.

[35] Xiao L, Bursi OS, Wang M, et al. Metamaterial beams with negative stiffness absorbers and rotation : band-gap behavior and band-gap merging. Eng Struct 2023;280:115702. https://doi.org/10.1016/j.engstruct.2023.115702.

[36] Li Q, Sheng M. An improved method for bandgap calculation of a locally resonant plate with multi-periodic of multiple degree-of-freedom resonators. J Appl Phys 2021;129:. https://doi.org/10.1063/5.0045424.

[37] Liang F, Xu WH, Chen ZQ (2023) Flexural–torsional vibration reduction of an eccentric phononic crystal pipe conveying fluid. J Fluids Struct 120:103904. https://doi.org/10.1016/j.jfluidstructs.2023.103904.

[38] Wu J, Sun Y, Su M, Zhu H. Fluid-structure interaction and band gap analysis of periodic composite liquid-filled pipe. Compos Struct 2023;304:116444. https://doi.org/10.1016/j.compstruct.2022.116444.

[39] Liang F, Yang X (2020) Wave properties and band gap analysis of deploying pipes conveying fluid with periodic varying parameters. Appl Math Model 77:522–538. https://doi.org/10.1016/j.apm.2019.07.064.

[40] Yu H, Liang F, Qian Y, et al (2021) Phononic band gap and free vibration analysis of fluid-conveying pipes with periodically varying cross-section. Appl Sci 11:1–18.

[41] Ni A, Shi Z, Meng Q, Lim CW. A novel buried periodic in-filled pipe barrier for Rayleigh wave attenuation: Numerical simulation, experiment and applications. Eng Struct 2023;297:116971. https://doi.org/10.1016/j.engstruct.2023.116971.

[42] Liang F, Chen Y, Gong J, Qian Y (2022) Vibration self-suppression of spinning fluid-conveying pipes composed of periodic composites. Int J Mech Sci 220:107150. https://doi.org/10.1016/j.ijmecsci.2022.107150.

[43] Wu JH, Zhu HZ, Sun YD, et al. Torsional Wave Propagation and Vibration Reducing of Phononic Crystal Pipe with Periodic Torsional Support. J Press Vessel Technol Trans ASME 2023;145:1–9. https://doi.org/10.1115/1.4055066.

[44] Liang F, Chen Z, Xu W (2023) Vibration isolation of a self-powered piezoelectric pipe conveying fluid composed of laminated fiber-reinforced composites. Appl Ocean Res 138:103664. https://doi.org/10.1016/j.apor.2023.103664.

[45] Bu Y, Tang Y, Ding Q. Novel vibration self-suppression of periodic pipes conveying fluid based on acoustic black hole effect. J Sound Vib 2023;567:118077. https://doi.org/10.1016/j.jsv.2023.118077.

[46] Geng Q, Zhao G, Yang X, et al (2024) Flexural vibration suppression behavior of sleeved phononic crystal pipes in thermal environment. Eng Struct 309:118011. https://doi.org/10.1016/j.engstruct.2024.118011.

[47] Plisson J, Pelat A, Gautier F, et al. Experimental evidence of absolute bandgaps in phononic crystal pipes. Appl Phys Lett 2020;116:201902. https://doi.org/10.1063/5.0007532.

[48] Fernandes R, El-borgi S, Yazbeck R, et al. Non-dimensional analysis of the bandgap formation in a locally resonant metamaterial pipe conveying fluid. Appl Math Model 2022;106:241–258. https://doi.org/10.1016/j.apm.2021.12.036.

[49] Liang F, Chen Y, Kou H, Qian Y. Hybrid Bragg-locally resonant bandgap behaviors of a new class of motional two-dimensional meta-structure. Eur J Mech / A Solids 2023;97:104832. https://doi.org/10.1016/j.euromechsol.2022.104832.

[50] Matos PHMC, Neves DA, Vieira SC, et al. Analytical and experimental investigation of flexural waves in horizontal pipes conveying two-phase periodic intermittent flow. Appl Acoust 2022;192:108714. https://doi.org/10.1016/j.apacoust.2022.108714.

[51] El-borgi S, Alrumaihi A, Rajendran P, et al. Model updating of a scaled piping system and vibration attenuation via locally resonant bandgap formation. Int J Mech Sci 2021;194:106211. https://doi.org/10.1016/j.ijmecsci.2020.106211.

[52] Iqbal M, Kumar A, Bursi OS. Lateral flexural vibration reduction in a periodic piping system enhanced with two-degrees-of-freedom resonators. Proc Inst Mech Eng Part L J Mater Des Appl 2021;0:1–11. https://doi.org/10.1177/14644207211027603.

[53] Lyu X, Chen F. Ultra-thin Piezoelectric Lattice for Vibration Suppression in Pipe Conveying Fluid. Acta Mech Solida Sin 2020;33:770–780. https://doi.org/10.1007/s10338-020-00174-z.

[54] Liu J, Yu D, Zhang Z, et al. Flexural Wave Bandgap Property of a Periodic Pipe with Axial Load and Hydro-Pressure. Acta Mech Solida Sin 2019;32:173–185. https://doi.org/10.1007/s10338-018-0070-2.

[55] Yu D, Wen J, Shen H, Wen X (2012) Propagation of steady-state vibration in periodic pipes conveying fluid on elastic foundations with external moving loads. Phys Lett A 376:3417–3422. https://doi.org/10.1016/j.physleta.2012.09.041.

[56] Sciutteri S, Russillo AF, Santoro R, et al (2024) An inerter-based concept of locally resonant fluid-conveying pipe. Eur J Mech A/Solids 106:105316. https://doi.org/10.1016/j.euromechsol.2024.105316.

[57] Wu J, Sun Y, Su M, et al. Band gap analysis of composite fluid-filled pipe with periodically axial support or dynamic vibration absorbers. Mech Adv Mater Struct 2022;0:1–9. https://doi.org/10.1080/15376494.2022.2088908.

[58] Frahm, H. Device for damping vibrations of bodies. US Patent US 989958A (1909).

[59] Ormondroyd J, Den Hartog JP. The theory of the dynamic vibration absorber. Trans Am Soc.Mech Eng 1928;50, 9–22.

[60] Su N, Chen Z, Xia Y, Bian J (2024) Hybrid analytical H-norm optimization approach for dynamic vibration absorbers. Int J Mech Sci 264:108796.

https://doi.org/10.1016/j.ijmecsci.2023.108796.

[61] Warburton GB. Optimum absorber parameters for various combinations of response and excitation parameters. Earthq Eng Struct D 1982;10, 381–401.

[62] Warburton GB, Ayorinde EO. Optimum absorber parameters for simple systems. Earthq Eng Struct D 1980;8, 197–217.

[63] Bisegna P, Caruso G (2012) Closed-form formulas for the optimal pole-based design of tuned mass dampers. J Sound Vib 331:2291–2314. https://doi.org/10.1016/j.jsv.2012.01.005.

[64] Argenziano M, Faiella D, Carotenuto AR, et al (2022) Generalization of the Den Hartog model and rule-of-thumb formulas for optimal tuned mass dampers. J Sound Vib 538:117213. https://doi.org/10.1016/j.jsv.2022.117213.

[65] Murugan Jaya M, Ceravolo R, Matta E, Fragonara LZ. A resonating lattice TMD to reduce pipeline vibrations. In American Society of Mechanical Engineers, Pressure Vessels and Piping Division (Publication) PVP (2018).

[66] Frans R, Arfiadi Y. Designing optimum locations and properties of MTMD systems. In Procedia Engineering 892–898 (2015).

[67] Arfiadi Y, Hadi MNS. Optimum placement and properties of tuned mass dampers using hybrid genetic algorithms. Int J Optim Civ Eng 2011;1, 167–187.

[68] Norris MA, Ptak KR, Zamora BA, Hart JD. Implementation of Tuned Vibration Absorbers for Above Ground Pipeline Vibration Control. 3rd International Pipeline Conference, IPC2000-115.

[69] Hart DJ, Sause R, Ford GW Brown LD. Pipeline vibration damper. US Patent US 5193644A (1991).

[70] Song GB, zhang P, Li LY, Singla M. Vibration control of a pipeline structure using pounding tuned mass damper. J Eng Mech 2016;142:1–10.

[71] Barutzki F, Gurr-Beyer C, Hinz G, Kerkhof K, Schwenkkros J. Identifcation and Reduction of Piping Vibrations under Diferent Conditions. VCE Vienna Consulting Engineers ZT GmbH, Vienna.

[72] Bursi OS, Filippo R, Salandra V La, et al. Probabilistic seismic analysis of an LNG subplant. J Loss Prev Process Ind 2018;53:45–60. https://doi.org/10.1016/j.jlp.2017.10.009.

[73] Floquet G. Sur les équations différentielles linéaires à coefficients périodiques. Ann Sci l'´Ecole Norm Sup´erieure 1883;12:47–88.

[74] Bloch F. Über die Quantenmechanik der Elektronen in Kristallgittern. Zeitschrift für Phys 1928;52:555–600. https://doi.org/https://doi.org/10.1007/BF01339455.

[75] Iqbal M, Kumar A (2023) Analysis of bending waves and parametric influence on band gaps in periodic track structure. Mater Today Proc. https://doi.org/10.1016/j.matpr.2023.08.364.

[76] Ansys® Academic Research Version 2020 R2, ANSYS, Inc. www. ansys. com.

[77] Kumar RK, Kumar A (2023) Vibration attenuation of a beam supporting an unbalanced rotor using nonlinear energy sink. J Brazilian Soc Mech Sci Eng 6:1–14. https://doi.org/10.1007/s40430-023-04064-6.

[78] De-Jong KA. Analysis of the behavior of a class of genetic adaptive systems. Ph.D. Thesis, University of Michigan, 1975.

[79] Goldberg DE Genetic Algorithms in Search, Optimization and Machine Learning (Addison-Wesley Publishing Company, 1989).

[80] Murugan Jaya M Vibration monitoring and control of industrial structures', PhD Thesis, Politecnico di Torino, 2020.

[81] Chopra AK Dynamics of structures, 3rd ed. (Prentice Hall, 2006)